Parkinson's disease-linked *D620N VPS35* knockin mice manifest tau neuropathology and dopaminergic neurodegeneration

Xi Chen[a], Jennifer K. Kordich[a], Erin T. Williams[a], Nathan Levine[a], Allyson Cole-Strauss[b], Lee Marshall[a], Viviane Labrie[a,c], Jiyan Ma[a], Jack W. Lipton[b], and Darren J. Moore[a,1]

[a]Center for Neurodegenerative Science, Van Andel Research Institute, Grand Rapids, MI 49503; [b]Department of Translational Science and Molecular Medicine, Michigan State University, Grand Rapids, MI 49503; and [c]Division of Psychiatry and Behavioral Medicine, College of Human Medicine, Michigan State University, Grand Rapids, MI 49503

Mutations in the *vacuolar protein sorting 35 ortholog* (*VPS35*) gene represent a cause of late-onset, autosomal dominant familial Parkinson's disease (PD). A single missense mutation, D620N, is considered pathogenic based upon its segregation with disease in multiple families with PD. At present, the mechanism(s) by which familial *VPS35* mutations precipitate neurodegeneration in PD are poorly understood. Here, we employ a germline *D620N VPS35* knockin (KI) mouse model of PD to formally establish the age-related pathogenic effects of the D620N mutation at physiological expression levels. Our data demonstrate that a heterozygous or homozygous D620N mutation is sufficient to reproduce key neuropathological hallmarks of PD as indicated by the progressive degeneration of nigrostriatal pathway dopaminergic neurons and widespread axonal pathology. Unexpectedly, endogenous D620N VPS35 expression induces robust tau-positive somatodendritic pathology throughout the brain as indicated by abnormal hyperphosphorylated and conformation-specific tau, which may represent an important and early feature of mutant VPS35-induced neurodegeneration in PD. In contrast, we find no evidence for α-synuclein–positive neuropathology in aged *VPS35* KI mice, a hallmark of Lewy body pathology in PD. D620N VPS35 expression also fails to modify the lethal neurodegenerative phenotype of human A53T-α-synuclein transgenic mice. Finally, by crossing *VPS35* KI and null mice, our data demonstrate that a single *D620N VPS35* allele is sufficient for survival and early maintenance of dopaminergic neurons, indicating that the D620N VPS35 protein is fully functional. Our data raise the tantalizing possibility of a pathogenic interplay between mutant VPS35 and tau for inducing neurodegeneration in PD.

Parkinson's disease | retromer | animal model | neurodegeneration | tau

Parkinson's disease (PD) is a common neurodegenerative movement disorder that typically occurs in a sporadic manner and is considered to result from a complex interaction between genetic and environmental risk factors together with age (1–3). A small proportion of PD cases are inherited (5–10%) and are known to be caused by mutations in at least 13 genes (1). Among these familial cases, mutations in the *vacuolar protein sorting 35 ortholog* (*VPS35, PARK17*, Online Mendelian Inheritance in Man 614203) gene were recently identified to cause a late-onset, autosomal-dominant form of PD (4, 5). A single heterozygous missense mutation, Asp620Asn (D620N), has been shown to segregate with disease in large PD kindreds and is found in individual PD subjects worldwide (6). Although additional rare *VPS35* variants may also be linked to PD (i.e., P316S, R524W, I560T, H599R, and M607V), the D620N mutation is considered the only authentic pathogenic mutation identified to date (6). *VPS35* mutations represent the second most common cause of late-onset familial PD after *LRRK2* mutations and give rise to a disease spectrum with clinical symptoms and neuroimaging phenotypes similar to sporadic PD (4–7). However, the neuropathology associated with *VPS35* mutations in PD is not yet clear

since only a single D620N mutation carrier has been evaluated at autopsy but with the notable exception of key PD-relevant brain regions (i.e., substantia nigra, locus ceruleus, or any brainstem area) (7). Outside of these areas, *VPS35* mutation carriers lack extranigral α-synuclein–positive Lewy body pathology (7), a characteristic hallmark of PD brains. The mechanism by which dominantly inherited mutations in *VPS35* induce neuropathology and neurodegeneration in PD remains enigmatic.

VPS35 encodes a core component of the retromer complex, which is important for the sorting and recycling of endosomal protein cargo to the *trans*-Golgi network (TGN) or plasma membrane (8–12). The pentameric retromer complex consists of a core trimeric cargo-selective complex formed by the VPS35, VPS26, and VPS29 subunits that recognize and bind cargo and a sorting nexin dimer that mediates membrane recruitment and curvature (9, 13). A small proportion of the retromer binds to and recruits the pentameric Wiskott–Aldrich syndrome and SCAR homolog (WASH) complex (i.e., FAM21, WASH1, strumpellin, CCDC53, and KIAA1033) to endosomal membranes, to facilitate the formation of actin patches required for cargo partitioning into distinct domains for sorting (9, 14). Retromer sorts cargo from endosomes to the TGN, including the cation-independent mannose

NEUROSCIENCE

6-phosphate receptor (CI-MPR), sortilin 1 and SorLA, whereas the glucose transporter (GLUT1), ATG9A, and AMPA receptors (GluR1 and GluR2) are alternatively sorted to the plasma membrane (9, 12). While the D620N mutation in VPS35 does not influence the stability, assembly, or subcellular localization of the retromer, its only known molecular defect is an impaired association with the WASH complex via a diminished interaction with the FAM21 subunit, which is suggested to induce the abnormal sorting of select cargo (i.e., ATG9A, CI-MPR, and GluR1) in cultured cells (15–20). Whether these putative mechanisms extend to the mammalian brain and are important for neuronal degeneration induced by D620N VPS35 in PD is not yet known.

Dominant missense mutations typically exert their pathogenic actions via a gain-of-function mechanism; however, in some cases mutations can manifest in a loss-of-function manner through dominant-negative or haploinsufficient mechanisms. The precise mechanism of action of familial *VPS35* mutations is unclear and animal models can often play an informative role in distinguishing such mechanisms. A number of rodent models have been developed to understand both the normal function of VPS35 in the brain and to formally evaluate the pathogenic effects of PD-linked mutations in relevant neuronal circuits and populations. While transgenic mice expressing human VPS35 variants have not been reported, the deletion of endogenous *VPS35* in KO mice results in embryonic lethality, suggesting a critical role for VPS35 in development (21–23). The lethality of *VPS35* KO mice indicates that the heterozygous D620N mutation is unlikely to manifest disease via a full loss-of-function mechanism. Recent studies demonstrate that heterozygous KO mice or conditional *VPS35*$^{DAT-Cre}$ KO mice are viable and exhibit the degeneration of dopaminergic neurons in the substantia nigra, a hallmark pathology of PD, indicating that VPS35 function is critical for normal dopaminergic neuronal health (21, 22). While intriguing, these KO mice fail to model the specific mechanisms by which familial *VPS35* mutations induce PD and are likely to develop additional neuropathological phenotypes and susceptibilities unrelated to PD etiology that may complicate the identification of disease mechanisms.

To evaluate the effects of *VPS35* mutations, we previously developed a viral-mediated gene transfer model in adult rats to formally demonstrate that the overexpression of human VPS35 harboring a D620N mutation in the nigrostriatal pathway is sufficient to induce dopaminergic neurodegeneration and axonal pathology (18). This transgenic rodent model is inconsistent with a simple loss-of-function effect for the D620N mutation, and neurodegeneration is most likely due to a gain-of-function or partial dominant-negative mechanism. However, certain caveats of this viral-based model include (*i*) the restricted expression of mutant VPS35 to specific neuronal populations (that preclude the brain-wide assessment of neuropathology), (*ii*) its relatively acute time course (i.e., 12 wk), (*iii*) the requirement for non-physiological transgene overexpression, and (*iv*) the small difference in neuropathology between WT and D620N VPS35 (18). In the present study, we report the development of *D620N VPS35* knockin (KI) mice as a model of familial PD. We evaluate the impact of the D620N mutation at physiological expression levels on the development of PD-like neuropathology with chronic aging and its potential relationship with the PD-linked protein α-synuclein, and we address the mechanism of action of this familial mutation. We provide evidence that endogenous D620N VPS35 expression in KI mice is sufficient to recapitulate the progressive degeneration of nigral dopaminergic neurons, a hallmark of PD, and unexpectedly induces widespread tau neuropathology and axonal damage. D620N VPS35 KI mice provide an important tool for understanding the pathophysiological mechanisms underlying PD.

Results

Generation and Molecular Characterization of *D620N VPS35* KI Mice.
We obtained a newly developed conditional *D620N VPS35* KI mouse line from The Jackson Laboratory (stock no. 021807)

originally developed by the Michael J. Fox Foundation, as recently reported (24). These conditional mice were developed by introducing a *loxP*-flanked WT minigene (consisting of a splice acceptor, WT VPS35 exons 15–17, and a polyA signal) downstream of intron 14 and replacing endogenous exon 15 (with a D620N mutant version) by homologous recombination in ES cells (Fig. 1*A*). WT VPS35 is expected to be expressed under normal conditions (via splicing to the minigene), but after Cre-mediated recombination D620N VPS35 is expressed from the endogenous allele (Fig. 1 *A* and *B*). Upon intercrossing of heterozygous floxed mice (*VPS35*$^{FLOX/WT}$) we were unable to recover homozygotes (*VPS35*$^{FLOX/FLOX}$) despite the expected frequency of WT and heterozygous mice, suggesting that floxed homozygotes are most
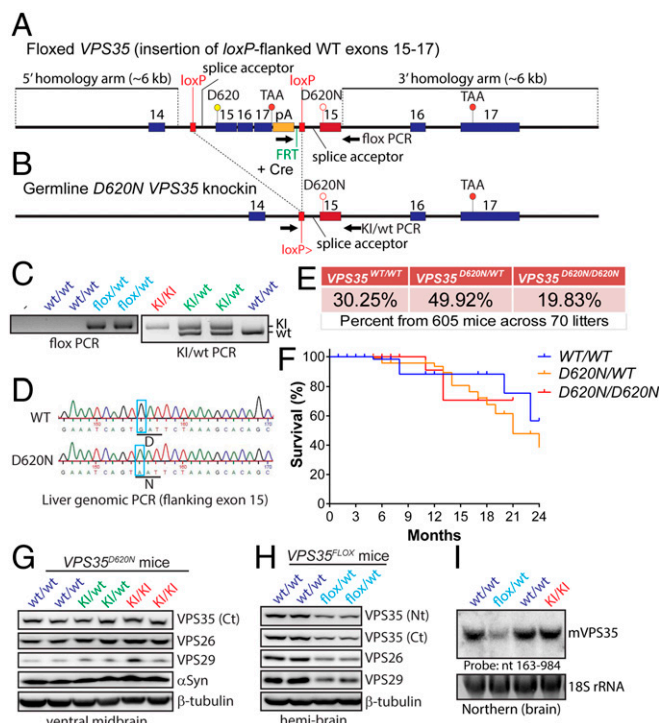

Fig. 1. Generation and molecular analyses of *D620N VPS35* KI mice. (*A*) Floxed VPS35 mice were developed by introducing a *loxP*-flanked WT "minigene" (containing a splice acceptor, WT VPS35 exons 15–17, and a polyA signal) downstream of intron 14 and replacing endogenous exon 15 (with a D620N mutant version) by homologous recombination in ES cells. WT VPS35 is expected to be expressed (via splicing to the minigene) but after Cre-mediated recombination D620N VPS35 is expressed from the targeted allele. (*B*) Germline *D620N* KI mice were developed by crossing floxed *VPS35* mice with CMV-Cre mice to remove the floxed WT minigene. KI mice contain a single *loxP* site and exon 15 harboring the D620N mutation. (*C*) PCR genotyping of tail genomic DNA for floxed VPS35 mice (*Left*) or germline VPS35 KI mice (*Right*) using PCR primers (arrows) as indicated in *A* or *B*. (*D*) Genomic PCR from liver DNA of germline *D620N/WT* and *WT/WT* mice using primers flanking exon 15. PCR products were cloned and sequenced to confirm the presence of the D620N mutation (GAT → AAT) in *D620N/WT* mice (*Lower*) compared with *WT/WT* mice (*Upper*). (*E*) Genotype frequencies from crosses of heterozygous (*VPS35*$^{D620N/WT}$) mice. Percentages are from 605 F1 progeny from 70 litters. (*F*) Kaplan–Meier survival curves of germline VPS35 KI mice were generated by monitoring cohorts of all genotypes (*VPS35*$^{WT/WT}$, n = 139; *VPS35*$^{D620N/WT}$, n = 302; *VPS35*$^{D620N/D620N}$, n = 125). (*G*) Western blot analysis of ventral midbrain extracts derived from 3-mo-old *D620N VPS35* KI mice using antibodies to endogenous VPS35 (Ct, residues 697–797), VPS26, VPS29, or β-tubulin. (*H*) Western blot analysis of hemibrains from floxed VPS35 mice using antibodies to VPS35 (Nt, residues 1–311 or Ct), VPS26, VPS29, or β-tubulin. (*I*) Northern blot analysis of total brain RNA using a VPS35-specific DNA probe (nucleotides 163–984) confirms normal VPS35 mRNA expression in the *D620N/D620N* KI mice but reduced VPS35 mRNA in *FLOX/WT* mice relative to their *WT/WT* littermates.

likely embryonic-lethal due to compromised VPS35 expression from the conditional allele. Notably, homozygous deletion of VPS35 in mice is embryonic-lethal (23). As such, germline D620N KI mice were developed by crossing $VPS35^{FLOX/WT}$ mice to CMV-Cre transgenic mice to remove the floxed WT minigene (Fig. 1 A and B). The resulting heterozygous KI mice ($VPS35^{D620N/WT}$) were intercrossed to produce cohorts of $VPS35^{WT/WT}$, $VPS35^{D620N/WT}$, and $VPS35^{D620N/D620N}$ littermate mice for subsequent age-dependent analysis. KI mice contain a single *loxP* site and exon 15 harboring the D620N mutation (Fig. 1B). PCR genotyping and genomic sequencing of the targeted exon 15 confirm correct gene targeting and the presence of the D620N mutation in KI mice (Fig. 1 C and D). Notably, heterozygous $VPS35^{D620N/WT}$ and homozygous $VPS35^{D620N/D620N}$ mice are viable, fertile, normal in appearance, produce genotypes at the expected frequency (Fig. 1E), and display normal survival up to 24 mo of age (Fig. 1F). Western blot analysis of ventral midbrain extracts from $VPS35^{D620N/D620N}$, $VPS35^{D620N/WT}$, and WT mice reveals normal levels of endogenous VPS35 as well as the retromer subunits VPS26 and VPS29 (Fig. 1G), confirming normal expression of VPS35 from the mutant allele and no effect of the D620N mutation on retromer stability. Similar experiments on hemibrains from conditional $VPS35^{FLOX/WT}$ mice indicate a ~50% reduction of VPS35 protein levels, as well as a corresponding reduction of VPS26 and VPS29, demonstrating that the floxed WT minigene compromises VPS35 expression from this conditional allele (Fig. 1H). Normal VPS35 mRNA expression levels and splicing in brains of $VPS35^{D620N/D620N}$ mice are also confirmed by Northern blot analysis of total RNA derived from brain (Fig. 1I). In contrast, we observe ~50% reduced VPS35 mRNA levels in the brains of $VPS35^{FLOX/WT}$ mice (Fig. 1I) consistent with Western blot data (Fig. 1H). Therefore, the conditional $VPS35^{FLOX/WT}$ mice are equivalent to heterozygous VPS35 null mice due to disrupted expression of VPS35 from the conditional allele. Collectively, the D620N mutation in VPS35 is well-tolerated in mice and does not influence retromer stability or survival, suggesting that it is unlikely to function through a loss-of-function mechanism.

Modest Motor Deficits in *D620N VPS35* KI Mice. To evaluate the potentially deleterious impact of D620N VPS35 expression on motor behavior, we conducted open-field, rotarod, and gait analyses on $VPS35^{D620N/WT}$ and $VPS35^{D620N/D620N}$ mice compared with WT littermate control mice at different time points as the mice aged. $VPS35^{D620N/WT}$ and $VPS35^{D620N/D620N}$ mice do not exhibit altered body weight compared with $VPS35^{WT/WT}$ control mice (*SI Appendix*, Fig. S1). In the open-field quadrant, $VPS35^{D620N/WT}$ and $VPS35^{D620N/D620N}$ mice exhibit novelty-induced locomotor activity similar to that of WT mice at 3 and 13 mo of age, including measures of distance and speed (*SI Appendix*, Fig. S1). Rotarod analysis using an accelerating paradigm reveals similar motor balance, coordination, and learning between genotypes at 13 mo of age (*SI Appendix*, Fig. S1). Gait analysis assessed using a digital Catwalk system in D620N KI mice reveals a nonsignificant trend of gait impairment (i.e., average speed, limb swing speed, and cadence) in $VPS35^{D620N/D620N}$ mice at 6, 9, and 12 mo (*SI Appendix*, Fig. S1), whereas base of support (distance between front or hind paws) and paw print position (distance between right or left paws) are normal (*SI Appendix*, Fig. S1). Taken together, the expression of D620N VPS35 has a rather modest impact on motor function at advanced age.

D620N VPS35 Expression Induces Progressive Dopaminergic Neurodegeneration. To determine whether the expression of *D620N VPS35* in mice influences the integrity of the nigrostriatal dopaminergic pathway with age, cohorts of KI mice were aged up to 13 mo. The number of tyrosine hydroxylase (TH)-positive dopaminergic and total Nissl-positive neurons in the substantia nigra pars compacta (SNpc) of $VPS35^{D620N/WT}$, $VPS35^{D620N/D620N}$, and WT littermate mice were assessed using unbiased stereological counting methodology. The morphology of dopaminergic neuronal soma and their neurite projections appear grossly normal in

$VPS35^{D620N/WT}$ and $VPS35^{D620N/D620N}$ mice (Fig. 2A). At ~3 mo of age, $VPS35^{D620N/D620N}$ mice display a modest nonsignificant reduction of nigral dopaminergic neuronal number compared with their $VPS35^{D620N/WT}$ or WT littermates (Fig. 2B). Remarkably, at 13 mo of age, $VPS35^{D620N/D620N}$ mice exhibit a significant loss (38 ± 4.0%) of dopaminergic neurons, whereas $VPS35^{D620N/WT}$ mice also exhibit significant dopaminergic neuronal loss (31 ± 3.4%) relative to WT mice (Fig. 2C). The loss of TH-positive neurons is due to neuronal degeneration rather than to a loss of TH phenotype, as indicated by a corresponding significant loss of total Nissl-positive SNpc neurons in $VPS35^{D620N/D620N}$ (31 ± 3.5%) and $VPS35^{D620N/WT}$ (22 ± 2.6%) mice compared with WT mice (Fig. 2C). Unexpectedly, the density of TH-positive dopaminergic nerve terminals in the striatum of $VPS35^{D620N/WT}$ and $VPS35^{D620N/D620N}$ mice at 13 mo is normal compared with their WT littermates (*SI Appendix*, Fig. S2), suggesting a compensatory resprouting of the remaining dopaminergic axonal processes. To further examine the impact of D620N VPS35 expression on nigrostriatal pathway function, we monitored the levels of biogenic amines in the striatum of $VPS35^{D620N/WT}$, $VPS35^{D620N/D620N}$, and WT mice at 14 to 15 mo of age by HPLC with electrochemical detection. Consistent with the normal density of striatal dopaminergic nerve terminals, D620N VPS35 KI mice display normal levels of striatal dopamine and its metabolites [3,4-dihydroxyphenylacetic acid (DOPAC) and homovanillic acid (HVA)] as well as other biogenic amines including serotonin and norepinephrine (Fig. 2D). Dopamine and other biogenic amines are also normal in the prefrontal cortex and olfactory bulb (*SI Appendix*, Fig. S2), which receive projections from dopaminergic neurons in the ventral tegmental area. Dopamine and serotonin turnover in the striatum, prefrontal cortex, and olfactory bulb are not altered in the KI mice (*SI Appendix*, Fig. S2). Collectively, heterozygous and homozygous D620N KI mice develop robust and progressive substantia nigra dopaminergic neuronal degeneration with age, thereby recapitulating one of the major pathological hallmarks of PD.
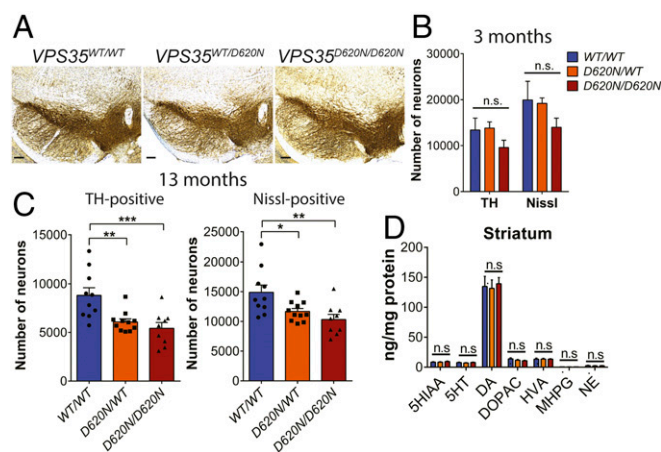

Fig. 2. Progressive loss of nigrostriatal pathway dopaminergic neurons in *D620N VPS35* KI mice. Unbiased stereological analysis of TH+ and Nissl+ neurons in the SNpc reveal dopaminergic neuronal loss in KI mice. (A) Representative images of TH immunostaining in the substantia nigra of 13-mo KI mice. (Scale bars: 500 μm.) (B and C) Stereological quantitation of dopaminergic (TH-positive) and total Nissl-positive neurons in the substantia nigra of (B) 3-mo-old (n = 4 animals per genotype) and (C) 13-mo-old (n = 9 to 11 animals per genotype) D620N VPS35 KI mice. Bars represent mean ± SEM, *P < 0.05, **P < 0.01 or ***P < 0.001 by one-way ANOVA with Bonferroni's post hoc test. (D) Striatal catecholamine levels in KI mice at 15 mo assessed by HPLC-ECD. Bars represent the mean ± SEM (n = 10 animals per genotype). Concentrations of biogenic amines are expressed in nanograms per milligram of protein. Levels of dopamine (DA) and its metabolites DOPAC and HVA as well as 5-HT and its metabolites 5-HIAA and norepinephrine (NE) are shown.

Axonal Damage in *D620N VPS35* KI Mice. Since the neuropathological spectrum associated with familial *VPS35* mutations in PD is not yet clear, we next evaluated the development of PD-related neuropathology using a number of classical markers of neuronal damage and degeneration. Reactive gliosis consistently accompanies neuronal degeneration in PD and other neurodegenerative diseases. However, evidence for astrogliosis (GFAP) or microgliosis (Iba1) is not observed throughout the brains of $VPS35^{D620N/WT}$ and $VPS35^{D620N/D620N}$ mice at 13 mo (*SI Appendix*, Fig. S3). Axonal pathology was next evaluated using either immunostaining for amyloid precursor protein (APP), a sensitive marker of axonal damage, or staining with Gallyas silver, which specifically labels degenerating neuronal soma and processes. $VPS35^{D620N/WT}$ and $VPS35^{D620N/D620N}$ mice at 13 mo display the accumulation of spherical axonal inclusions containing APP as well as increased cytoplasmic APP within neurons of the striatum and substantia nigra (Fig. 3A). $VPS35^{WT/WT}$ mice do not develop these abnormalities. The accumulation of APP-positive axonal inclusions suggests that the expression of D620N VPS35 may also promote axonal degeneration. Gallyas silver staining of striatum and substantia nigra sections from 13-mo-old $VPS35^{D620N/WT}$ and $VPS35^{D620N/D620N}$ mice reveals neurite degeneration, as indicated by the silver/black staining of neurites (Fig. 3B). Quantitation of silver-positive neurites in the striatum confirms a significant increase in neurite degeneration in $VPS35^{D620N/WT}$ and $VPS35^{D620N/D620N}$ mice compared with WT mice (Fig. 3C). No evidence of neurite degeneration is observed in D620N KI mice at 3 mo of age (see Fig. 9E). Neurite degeneration is more prominently detected outside of the nigrostriatal pathway, with extensive silver-positive axonal and neuronal degeneration present in the hippocampal CA1-3 region, cerebellum, and brainstem (but not the cortex) of $VPS35^{D620N/WT}$ and $VPS35^{D620N/D620N}$ mice at 13 mo (*SI Appendix*, Fig. S4). $VPS35^{WT/WT}$ mice display minimal silver-positive neurites or neurons (Fig. 3 B and C and *SI Appendix*, Fig. S4). Collectively, our data reveal marked and widespread axonal pathology in the brains of D620N VPS35 KI mice.

Accumulation of Abnormal Tau Protein in Brains of *D620N VPS35* KI Mice. To further determine the pathological consequences of *VPS35* mutations in vivo, and given the prominent axonal pathology observed in KI mice (Fig. 3), we next assessed alterations in the microtubule-associated protein tau (MAPT). Tau normally localizes to axonal processes via its interaction with microtubules but can dissociate from axons to form intraneuronal neurofibrillary tangles (NFTs) consisting of paired helical filament tau, the hallmark pathology of neurodegenerative tauopathies such as Alzheimer's disease (25, 26). Notably, some PD brains harboring *LRRK2* mutations as well as a number of LRRK2 rodent models can manifest tau-positive neuropathology (27–29), whereas common variation in the *MAPT* gene is associated with increased PD risk (30). Given that NFTs contain tau species that are abnormally hyperphosphorylated at multiple sites and adopt abnormal conformations (25, 26, 31), we used antibodies that detect specific disease-associated phosphorylation (AT8, PHF1, or CP13) or conformational (MC1) epitopes of tau. Intriguingly, we find evidence for prominent tau-positive neuropathology in the D620N VPS35 KI mice. Tau abnormalities are prominent by 13 mo of age in $VPS35^{D620N/WT}$ and $VPS35^{D620N/D620N}$ mice using antibodies to pSer202/pThr205 (AT8) and abnormal conformation-specific (MC1) tau epitopes in the CA1–CA3 subregions of the hippocampus involving the accumulation of tau in the soma and dendritic compartments of neurons (Fig. 4). Additional phospho-specific tau epitopes, pSer202 (CP13) and pSer396/Ser404 (PHF1), also accumulate but to a lesser extent in the hippocampal subregions of $VPS35^{D620N/WT}$ and $VPS35^{D620N/D620N}$ mice compared with WT mice (*SI Appendix*, Fig. S5). Tau abnormalities (AT8 and MC1) are detected most prominently in the cortex, hippocampus, and cerebellum of aged $VPS35^{D620N/WT}$ and $VPS35^{D620N/D620N}$ mice, followed by marked tauopathic changes in brainstem and ventral midbrain, and only modest tau pathology in the striatum (*SI Appendix*, Fig. S6). Somatodendritic tau pathology is generally more prominent in $VPS35^{D620N/WT}$ mice relative to $VPS35^{D620N/D620N}$ mice, compared with general background staining observed in $VPS35^{WT/WT}$ mice (Fig. 4 and *SI Appendix*, Figs. S5 and S6).

Immunofluorescent colocalization studies in the hippocampus further reveal that abnormal tau accumulation (AT8 and MC1) is largely confined to the dendritic arbor of pyramidal neurons (i.e., stratum oriens, radiatum, and moleculare layers) and to occasional NeuN-positive neuronal soma in the stratum oriens and pyramidale layers of KI mice at 13 mo (Fig. 5A). Quantitation of AT8 and MC1 fluorescence intensity levels in the hippocampal CA1 and CA3 subregions confirms a significant increase of tau pathology in the $VPS35^{D620N/WT}$ and $VPS35^{D620N/D620N}$ mice compared with WT mice (Fig. 5B). In the substantia nigra, the significant accumulation of total (Tau5) and abnormal (AT8 and MC1) tau is observed specifically in TH-positive dopaminergic neurons of *D620N* KI mice at 13 mo of age (Fig. 6) and is detectable as early as 3 mo of age (*SI Appendix*, Fig. S5). Throughout the brains of D620N KI mice, we do not generally find evidence for tau-positive NFTs, inclusions, or neuritic pathology containing fibrillar forms of tau (Figs. 4–6 and *SI Appendix*, Figs. S5 and S6), suggesting instead that abnormal tau most likely accumulates rather than aggregates in somatodendritic compartments most consistent with earlier forms of "pre-tangle" pathology (25, 31).

To further explore the aggregation state of tau in D620N KI brains, we conducted biochemical studies to determine the steady-state levels, solubility, or abnormal phosphorylation of tau. At 13 mo of age, 1% Triton-soluble extracts derived from D620N KI mice fail to reveal consistent alterations in the steady-state levels (Tau5), phosphorylation (AT8), or abnormal conformation (MC1) of tau protein in the ventral midbrain and hippocampus of $VPS35^{D620N/WT}$ and $VPS35^{D620N/D620N}$ mice (*SI*
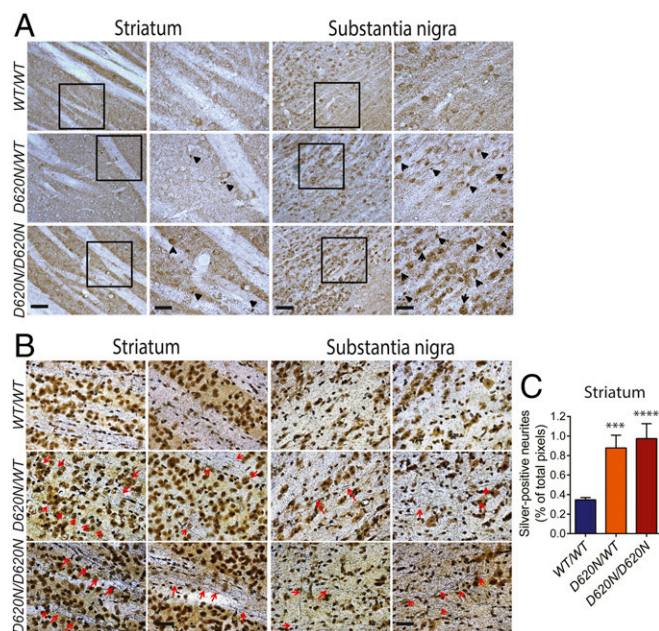

Fig. 3. Axonal damage in *D620N VPS35* KI mice. Representative photomicrographs of striatum and substantia nigra from 13-mo-old $VPS35^{D620N/WT}$, $VPS35^{D620N/D620N}$, and control $VPS35^{WT/WT}$ mice indicating (A) APP immunohistochemistry revealing APP-positive spheroids (*black arrowheads*), a marker of axonal damage. (Scale bars: 100 µm.) Insets show high-power images of the boxed regions. (Scale bars: 50 µm.) (B) Gallyas silver staining revealing degenerating neuritic processes (*red arrows*). (Scale bar: 50 µm.) (C) Bar graph indicating quantitation of silver-positive black neurites in the striatum. Data are expressed as the percent of total pixels per image (mean ± SEM, *n* = 5 or 6 animals per genotype). ***P* < 0.001 or *****P* < 0.0001 by one-way ANOVA with Bonferroni's post hoc test compared with *WT/WT* mice.
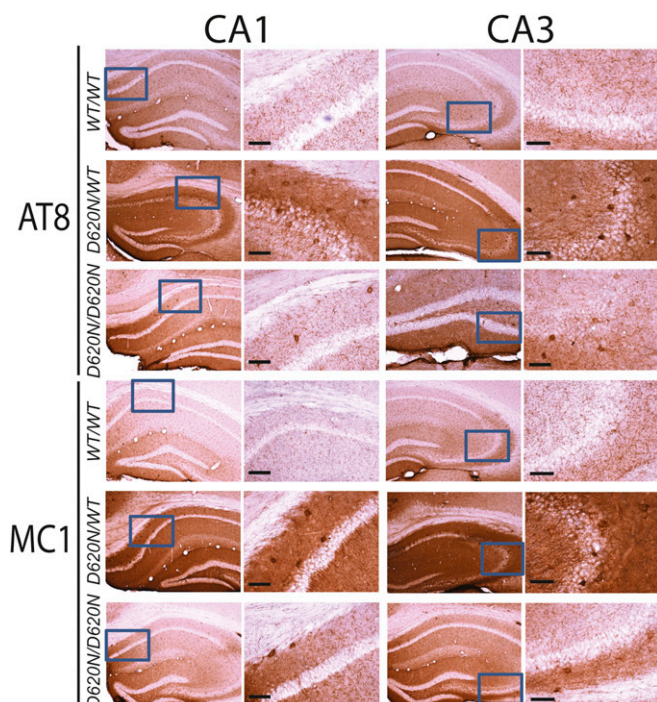
Fig. 4. Hippocampal tau abnormalities in *D620N VPS35* KI mice. Representative photomicrographs of hippocampus from 13-mo-old *VPS35^D620N/WT^*, *VPS35^D620N/D620N^*, and control *VPS35^WT/WT^* mice indicating immunohistochemical staining with antibodies to phosphorylation-specific tau (AT8) or abnormal conformation-specific tau (MC1). AT8- and MC1-positive immunoreactivity, including abnormal somatodendritic labeling, is markedly increased in the hippocampus of *D620N/WT* and *D620N/D620N* mice compared with WT mice. Insets represent high-power images from the boxed regions in the hippocampal CA1 and CA3 subregions. (Scale bars: 100 µm.)

Appendix, Fig. S7). A central feature of human tauopathies is the loss of tau solubility and the accumulation of hyperphosphorylated tau that can be isolated from brain tissue with sarkosyl extraction (25). Accordingly, sequential detergent extraction (low-salt-soluble, 1% Triton X-100–soluble, 1% sarkosyl-soluble, and sarkosyl-insoluble fractions) was conducted on brain regions with prominent tau pathology (hippocampus and cerebellum) from D620N KI mice at 13 mo. In general, D620N VPS35 expression does not robustly or consistently alter the detergent solubility of endogenous tau or significantly alter AT8 levels across fractions (*SI Appendix*, Fig. S7), consistent with the absence of NFTs in the KI mice (Figs. 4–6).

To explore the potential mechanism of tau accumulation in the D620N KI mice, we conducted similar studies in *VPS35^FLOX/WT^* mice with diminished VPS35 expression that serve as heterozygous KO mice (refer to Fig. 1*H*). Abnormal tau (AT8 and MC1) does not accumulate in hippocampal subregions of *VPS35^FLOX/WT^* mice compared with their *VPS35^WT/WT^* littermate mice at 12 mo of age (*SI Appendix*, Fig. S8). These data demonstrate that VPS35 deficiency is not sufficient to induce the accumulation of abnormal tau and suggest that tau pathology in D620N KI mice does not manifest via a simple loss-of-function mechanism.

Retromer Subunit Assembly and Levels in Brains of *D620N VPS35* KI Mice. Western blot analyses of ventral midbrain extracts from *VPS35^D620N/D620N^*, *VPS35^D620N/WT^*, and WT mice at 3 mo reveal normal levels of the cargo-selective complex subunits VPS35, VPS26, and VPS29 (Fig. 1*G*). Therefore, the D620N mutation does not obviously influence overall retromer stability. To evaluate the interaction of VPS35 with retromer complex subunits in the brain of D620N KI mice, we conducted coimmunoprecipitation (co-IP) assays with a VPS35-specific antibody using solu-

ble hemibrain extracts from *VPS35^D620N/D620N^* and WT mice. WT and D620N VPS35 interact robustly and equivalently with VPS26 in brain (Fig. 7*A*). However, we are unable to detect an interaction of WT or D620N VPS35 with the WASH complex subunits FAM21 and WASH1 (Fig. 7*A*). We could further confirm the equivalent interaction with retromer subunits VPS26A, VPS26B, and VPS29 by mass spectrometric analysis of VPS35 IPs from WT or D620N KI brains, but we are unable to detect any WASH complex subunits (Fig. 7*B*). Using similar co-IP assays, we can detect the robust interaction of V5-tagged WT VPS35 with endogenous WASH1 and FAM21 in HEK-293T cells and the marked impairment of both interactions with D620N VPS35 (Fig. 7*C*), as previously reported (16, 19). Our data suggest that endogenous VPS35 in the mouse brain does not appreciably interact with the WASH complex. Next, we conducted confocal colocalization studies to understand the pathogenic effects of the D620N mutation in dopaminergic neurons of the substantia nigra. Intriguingly, we find a marked significant reduction of VPS35 and WASH1 levels selectively in intact TH-positive dopaminergic neurons of both *VPS35^D620N/D620N^* and *VPS35^D620N/WT^* mice compared with their WT littermates at 3 mo (Fig. 7 *D* and *E*). These data suggest a selective retromer deficit (VPS35 and WASH complex) in nigral dopaminergic neurons due to the D620N mutation, whereas retromer levels and assembly are generally normal in the brains of KI mice (Figs. 1*G* and 7 *A* and *B*).
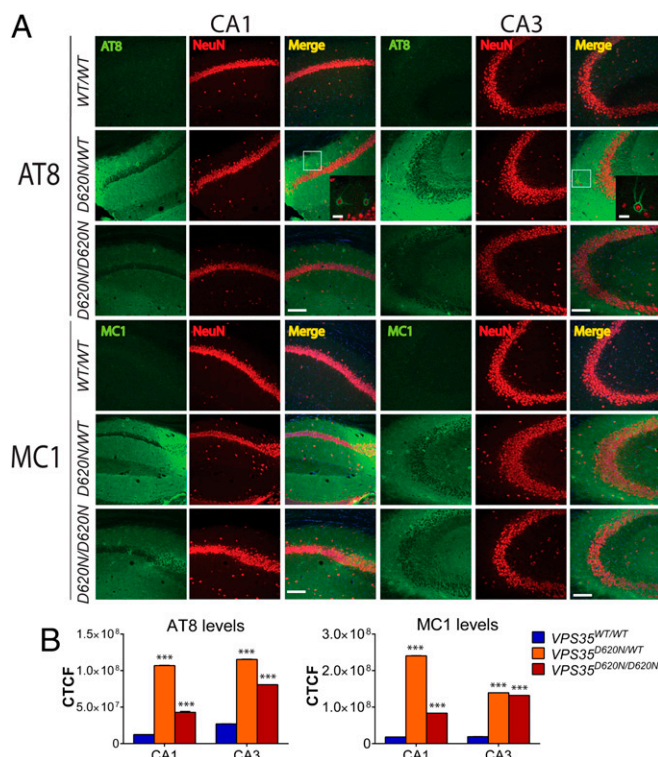

Fig. 5. Immunofluorescence analysis of tau in hippocampal CA1–CA3 subregions from *D620N VPS35* KI mice. (*A*) Immunofluorescent confocal colocalization analysis of hippocampal CA1 or CA3 from 13-mo-old *VPS35^D620N/WT^*, *VPS35^D620N/D620N^*, and control *VPS35^WT/WT^* mice colabeled with AT8 or MC1 tau antibodies (green) and the pan-neuronal marker NeuN (red). Merged images indicate AT8- and MC1-positive immunoreactivity mainly localized to neuritic processes of pyramidal neurons but also to the soma (boxed region and inset) of *D620N/WT* and *D620N/D620N* mice. Insets show high-power images of the boxed regions from merged images. (Scale bars: 15 µm.) (*B*) Bar graphs indicating CTCF values (mean ± SEM, n = 4 animals per group) of AT8 or MC1 fluorescence intensity in the CA1 or CA3 subregions. ***P < 0.001 by one-way ANOVA with Bonferroni's post hoc test compared with WT/WT mice.
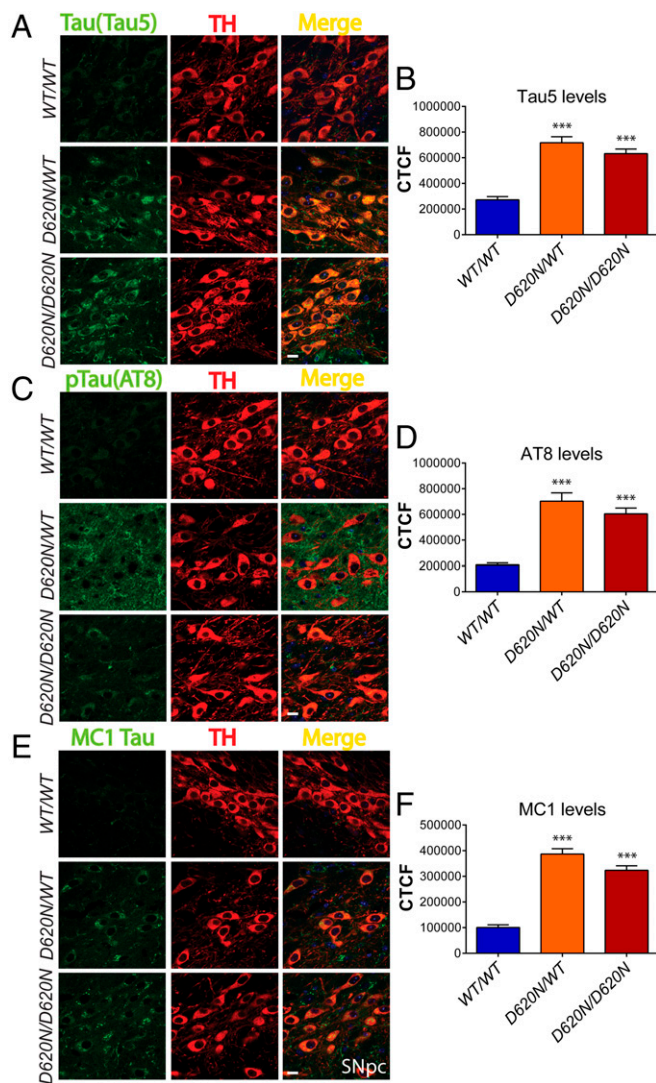
Fig. 6. Tau abnormalities in nigral dopaminergic neurons of *D620N VPS35* KI mice. Immunofluorescent confocal colocalization analysis of the SNpc from 13-mo-old *VPS35^{D620N/WT}*, *VPS35^{D620N/D620N}*, and control *VPS35^{WT/WT}* mice colabeled with (*A*) Tau5 (total tau), (*C*) AT8, or (*E*) MC1 antibodies (green) and the dopaminergic neuronal marker TH (red). Merged images indicate the accumulation of Tau5-, AT8-, and MC1-positive immunofluorescent signals within the somatodendritic compartment of nigral dopaminergic neurons of *D620N/WT* and *D620N/D620N* mice. (Scale bars: 15 μm.) Bar graphs indicating CTCF values (mean ± SEM, $n = 4$ animals per group) of (*B*) Tau5, (*D*) AT8, or (*F*) MC1 fluorescence intensity in TH-positive dopaminergic neurons. ***$P < 0.001$ by one-way ANOVA with Bonferroni's post hoc test compared with *WT/WT* mice.

Lack of α-Synuclein Pathology or Functional Interaction in *D620N VPS35* KI Mice. α-Synuclein plays a central role in the pathogenesis of PD, where it comprises a key component of Lewy pathology (30, 32–34). Prior studies have revealed a functional interaction of VPS35 and α-synuclein, whereby *VPS35* deletion in yeast and worm models can exacerbate human α-synuclein–induced toxicity (35), whereas α-synuclein accumulates in the brains of mice with *VPS35* depletion (21, 22). As such, we evaluated brains from aged D620N VPS35 KI mice for alterations in α-synuclein levels or aggregation. *VPS35^{D620N/WT}* and *VPS35^{D620N/D620N}* mice do not reveal consistent alterations in the levels, distribution, or morphology of phosphorylated Ser129-α-synuclein above background levels throughout the brain (*SI Appendix*, Fig. S9), a robust marker of pathological α-synuclein

specific to Lewy pathology in PD (36). Biochemical analyses of detergent-soluble (1% Triton X-100) extracts from the ventral midbrain of 13-mo-old D620N KI mice indicate normal steady-state levels and phosphorylation (Ser129) of α-synuclein (*SI Appendix*, Fig. S9), consistent with immunohistochemical data. Therefore, D620N KI mice lack evidence of α-synuclein accumulation or neuropathology, in contrast to *VPS35 KO* mice (21, 22).

To further explore a potential pathological interaction of VPS35 with α-synuclein, we crossed the D620N VPS35 KI mice with human A53T-αSyn transgenic mice (line G2-3), a robust and well-characterized model of α-synuclein–induced neurodegeneration (37). *VPS35^{D620N/D620N}* mice were first crossed with hemizygous A53T-αSyn mice to generate F1 progeny (i.e., *VPS35^{D620N/WT}* and *VPS35^{D620N/WT}/αSyn^{Tg}*) that were subsequently intercrossed to generate F2 cohorts for direct comparison (Fig. 8). A53T-αSyn transgenic mice display shortened lifespan largely owing to the robust degeneration of brainstem and spinal cord neurons leading to limb paralysis, autonomic dysfunction, and premature death (37). Accordingly, we assessed the impact of physiological D620N VPS35 expression on the survival of
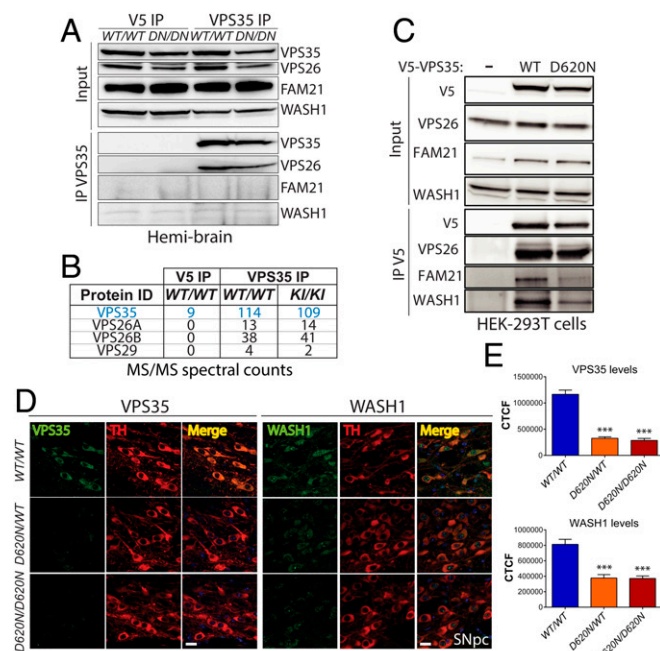

Fig. 7. Normal retromer assembly in brain but reduced VPS35 and WASH complex in dopaminergic neurons of *D620N VPS35* KI mice. (*A*) Hemibrain extracts from *D620N VPS35* KI and WT mice at 3 mo ($n = 2$ mice per genotype) were subjected to IP with anti-VPS35 antibody (or control anti-V5 IgG). Western blot analysis of IP and input fractions reveal equivalent interactions of endogenous WT and D620N VPS35 with retromer subunit VPS26, whereas WASH complex subunits (FAM21 and WASH1) are not detected. (*B*) LC-MS/MS analysis of anti-VPS35 IP (or anti-V5 IP) fractions from *A* reveal equivalent interactions of WT and D620N VPS35 with retromer subunits VPS26A, VPS26B, and VPS29 in mouse brain. WASH complex subunits are not detected. MS/MS spectral counts for each protein are shown. (*C*) HEK-293T cells expressing V5-tagged human VPS35 (WT or D620N) were subjected to IP with anti-V5 antibody, and IP and input fractions were probed for VPS26, FAM21, and WASH1. WT and D620N VPS35 interact equivalently with endogenous VPS26, whereas D620N VPS35 displays an impaired interaction with endogenous FAM21 and WASH1. (*D*) Immunofluorescent confocal colocalization analysis reveals markedly reduced levels of VPS35 and WASH1 selectively in nigral dopaminergic neurons (TH-positive) of 3-mo-old *D620N/WT* and *D620N/D620N* KI mice. (Scale bars: 15 μm.) (*E*) Bar graphs indicating CTCF values (mean ± SEM, $n = 4$ animals per group) of VPS35 or WASH1 fluorescence intensity in TH-positive dopaminergic neurons. ***$P < 0.001$ by one-way ANOVA with Bonferroni's post hoc test compared with *WT/WT* mice.
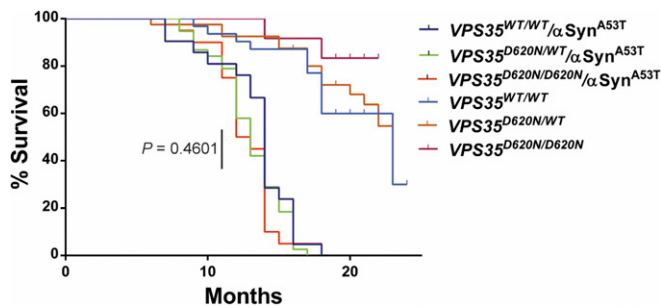
Fig. 8. Lethal neurodegenerative phenotype of human A53T-α-Syn transgenic mice is independent of D620N VPS35. Kaplan–Meier survival curves of A53T-α-Syn and A53T-α-Syn/VPS35 KI mice were generated by monitoring cohorts of all genotypes ($VPS35^{WT/WT}/\alpha Syn^{A53T}$, $n = 21$; $VPS35^{D620N/WT}/\alpha Syn^{A53T}$, $n = 48$; $VPS35^{D620N/D620N}/\alpha Syn^{A53T}$, $n = 23$) until mice had to be euthanized due to the onset of terminal disease. There is no significant difference between these three genotypes by log-rank (Mantel–Cox) test ($P = 0.4601$), as indicated. $VPS35^{WT/WT}$ ($n = 32$), $VPS35^{D620N/WT}$ ($n = 41$), and $VPS35^{D620N/D620N}$ ($n = 12$) mice exhibit normal survival up to 24 mo of age.

A53T-αSyn mice (Fig. 8). A53T-αSyn mice exhibit premature lethality occurring over a period of 8 to 18 mo of age. However, the survival of $VPS35^{D620N/WT}/\alpha Syn^{Tg}$ and $VPS35^{D620N/D620N}/\alpha Syn^{Tg}$ mice does not significantly differ from that of $VPS35^{WT/WT}/\alpha Syn^{Tg}$ mice. $VPS35^{D620N/WT}$ and $VPS35^{D620N/D620N}$ mice exhibit normal survival relative to $VPS35^{WT/WT}$ mice over 24 mo (Fig. 8). Our data indicate that the lethal neurodegenerative phenotype of A53T-αSyn transgenic mice is not influenced by endogenous D620N VPS35 expression, in contrast to simpler models with VPS35 depletion (35, 38). We next conducted preliminary experiments by unilaterally delivering mouse α-synuclein preformed fibrils (PFFs) to the striatum of 6-mo-old $VPS35^{D620N/D620N}$ and $VPS35^{WT/WT}$ mice to explore the impact of the D620N mutation on the development of α-synuclein pathology (SI Appendix, Fig. S10). At 30 d postinjection, we observe pSer129-α-synuclein–positive pathology localized to dopaminergic neurons of the ipsilateral substantia nigra of $VPS35^{WT/WT}$ mice; however, qualitatively similar α-synuclein pathology is also observed in $VPS35^{D620N/D620N}$ mice (SI Appendix, Fig. S10). These data suggest that the D620N mutation does not regulate the initial progression and propagation of α-synuclein pathology in the αSyn-PFF model. Taken together, these data fail to provide robust evidence for a pathological interaction of α-synuclein in the D620N VPS35 KI mouse model.

The D620N Mutation Supports Survival and Is Inconsistent with a Full Loss-of-Function Mechanism. Our data indicate that homozygous D620N VPS35 KI mice display a normal lifespan (Fig. 1F), in contrast to homozygous KO mice (and $VPS35^{FLOX/FLOX}$ mice; Fig. 1A) which are embryonic-lethal (23), suggesting that the D620N mutation is not likely to act via a loss-of-function mechanism. To further address this mechanism, we crossed $VPS35^{D620N/WT}$ mice with $VPS35^{FLOX/WT}$ mice (containing a single VPS35 null allele) (Fig. 1 A, H, and I) to create compound heterozygous $VPS35^{D620N/FLOX}$ progeny. These mice harbor a single D620N allele and a VPS35 null allele and exhibit ~50% VPS35 protein levels in the brain similar to $VPS35^{FLOX/WT}$ mice, as expected (Fig. 9A). Importantly, we find that the $VPS35^{D620N/FLOX}$ mice are viable, grossly normal, produced at the expected genotypic frequency (Fig. 9B), and exhibit normal survival over 24 mo (Fig. 9C). At ~3 mo, the $VPS35^{D620N/FLOX}$ mice display a normal number of substantia nigra dopaminergic neurons (Fig. 9D) and lack axonal pathology (Fig. 9E) relative to WT littermate mice. These data are in contrast to conditional KO mice with homozygous VPS35 deletion in DAT-positive neurons that develop robust dopaminergic neuronal loss at 2 to 3 mo of age (22). We further evaluated tau pathology in the $VPS35^{D620N/FLOX}$ mice at 24 mo of age. Both $VPS35^{D620N/WT}$ and $VPS35^{D620N/FLOX}$ mice markedly accumulate abnormal tau

(AT8 and MC1) in hippocampal subregions that is completely absent from $VPS35^{FLOX/WT}$ mice (Fig. 9F). The burden of tau pathology in the CA3 subregion is similar between $VPS35^{D620N/WT}$ and $VPS35^{D620N/FLOX}$ mice, whereas in the CA1 subregion of $VPS35^{D620N/FLOX}$ mice the accumulation of abnormal tau shifts from dendrites to the soma of pyramidal neurons (Fig. 9F). As compound heterozygous $VPS35^{D620N/FLOX}$ mice alone are sufficient for the development of tau pathology, these data suggest that D620N VPS35 can induce pathology irrespective of the presence of WT VPS35. Furthermore, VPS35 depletion in the $VPS35^{FLOX/WT}$ mice is not sufficient to induce tau pathology (Fig. 9F and SI Appendix, Fig. S8), implying that the D620N mutation impacts tau protein via a gain-of-function mechanism. Since $VPS35^{-/-}$ and $VPS35^{FLOX/FLOX}$ mice are embryonic-lethal (23), our data collectively demonstrate that a single copy of the D620N allele
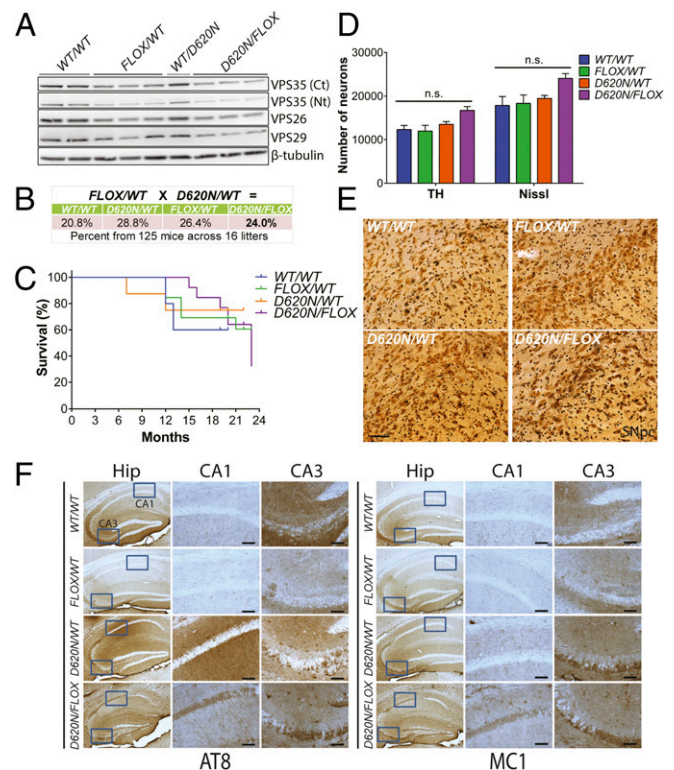

Fig. 9. A single D620N VPS35 allele is sufficient for normal survival, early dopaminergic neuronal health, and tau pathology. Heterozygous $VPS35^{D620N/WT}$ mice were crossed with $VPS35^{FLOX/WT}$ mice to create compound heterozygous $VPS35^{D620N/FLOX}$ progeny and their littermate controls. (A) Western blot analysis of hemibrain extracts derived from 3-mo-old VPS35 FLOX x D620N mice using antibodies to endogenous VPS35 (Nt, α1–311 or Ct, α697–797), VPS26, VPS29, and β-tubulin. (B) Genotype frequencies from crosses of heterozygous $VPS35^{D620N/WT}$ and $VPS35^{FLOX/WT}$ mice. Percentages are representative of 125 mice obtained from 16 litters. (C) Kaplan–Meier survival curves of VPS35 mice were generated by monitoring cohorts of all genotypes ($VPS35^{WT/WT}$, $n = 8$; $VPS35^{D620N/WT}$, $n = 8$; $VPS35^{FLOX/WT}$, $n = 13$; $VPS35^{D620N/FLOX}$, $n = 13$). (D) Stereological quantitation of dopaminergic neurons (TH-positive) and total Nissl-positive neurons in the SNpc of 3-mo-old VPS35 FLOX x D620N mice ($n = 5$ animals per genotype). Bars represent mean ± SEM, $P > 0.05$ by one-way ANOVA with Bonferroni's post hoc test. n. s., nonsignificant. (E) Representative images of Gallyas silver staining indicating the absence of neurite degeneration in the SNpc of 3-mo-old VPS35 FLOX x D620N mice. (Scale bar: 50 μm.) (F) Representative photomicrographs of hippocampus from 24-mo-old VPS35 FLOX x D620N mice indicating immunostaining with antibodies to AT8-tau or MC1-tau. AT8- and MC1-positive immunoreactivity is markedly increased in the CA1 and CA3 subregions of D620N/WT and D620N/FLOX mice compared with FLOX/WT or WT/WT mice. Insets represent high-power images from the boxed regions in CA1 and CA3 subregions. (Scale bars: 100 μm.)

(in compound $VPS35^{D620N/FLOX}$ mice) is sufficient for maintaining normal survival and early dopaminergic neuronal health in mice, indicating that D620N VPS35 is fully functional and highly unlikely to manifest disease via a loss-of-function mechanism (i.e., via a haploinsufficient or dominant-negative effect).

Discussion

Here, we report the development and phenotypic assessment of a germline *D620N VPS35* KI mouse model of PD with advancing age. We demonstrate that the expression of D620N VPS35 at endogenous levels is sufficient to induce the progressive degeneration of nigrostriatal pathway dopaminergic neurons, thereby recapitulating the major neuropathological hallmark of PD. KI mice develop rather modest motor deficits with age consistent with the normal density of striatal dopaminergic nerve terminals and dopamine levels. In addition, D620N VPS35 expression induces widespread axonal damage and tau-positive pathology throughout the brain, including within the substantia nigra. Tau pathology is characterized by the accumulation of abnormal hyperphosphorylated and conformational-specific epitopes within somatodendritic compartments and is most consistent with an early "pre-tangle" form of pathology. Heterozygous *VPS35* null mice to do not similarly develop tau pathology at advanced age. Surprisingly, we find no evidence for α-synuclein neuropathology in the D620N KI mice, a second pathological hallmark of PD. Furthermore, the D620N mutation is unable to modify the lethal neurodegenerative phenotype that develops in human A53T-αSyn transgenic mice or the initial development and propagation of α-synuclein pathology in an α-synuclein preformed fibril model of PD. Therefore, *VPS35* KI mice do not display an obvious pathological interaction with α-synuclein. At the molecular level, we find that the D620N VPS35 protein is stable within the brain and assembles normally within the retromer complex, but we find evidence of a retromer deficiency selectively within nigral dopaminergic neurons. Finally, we demonstrate that a single D620N allele is sufficient for normal survival and early dopaminergic neuronal health in *VPS35* null mice, indicating that the D620N VPS35 protein is fully functional and is unlikely to act via a loss-of-function mechanism. Taken together, our data demonstrate that the PD-linked dominant D620N mutation in *VPS35* is able to induce neuronal degeneration, axonal damage, and tau pathology, most likely via a gain-of-function mechanism. Our findings formally establish an important contribution of familial *VPS35* mutations to the development of PD.

D620N VPS35 KI mice are one of the first models of inherited monogenic PD that develop the robust and progressive degeneration of nigral dopaminergic neurons. Importantly, a heterozygous or homozygous D620N mutation produces similar neurodegenerative phenotypes in the KI mice. For tau pathology, the heterozygous KI mice even exhibit modestly enhanced pathology compared with homozygous mice. These data are consistent with a threshold effect of the D620N mutation for the development of neuropathology, rather than a gene dosage effect, which would lend support to a gain-of-function mechanism for this dominantly inherited mutation. This idea is supported by the viability and survival of homozygous D620N KI mice [in contrast to embryonic lethality in homozygous KO mice (23)] and by the ability of a single D620N allele to support normal survival in mice. Therefore, the D620N mutation does not compromise the overall function of VPS35, a finding supported by studies in yeast (18), and is not consistent with a simple loss-of-function mechanism. The observation that heterozygosity for the D620N mutation is sufficient for the development of fulminant pathology in the KI mice, whereas the viral-mediated overexpression of human D620N VPS35 can also produce similar phenotypes in rodents (18, 39), would tend to argue against a partial dominant-negative effect of this pathogenic variant. *VPS35* KO (heterozygous or conditional) mice also develop dopaminergic neurodegeneration (21, 22), although it is unclear whether this is a selective effect given that VPS35 is broadly expressed throughout the CNS and is critically required for

normal development (23). The molecular mechanism underlying the D620N mutation is not yet clear. Although our data support a gain-of-function effect as the most plausible mechanism for the D620N mutation in vivo, several studies have shown that this mutation impairs the interaction with and endosomal recruitment of the WASH complex by VPS35 in cell culture models (16, 19), a finding replicated in the present study. We demonstrate that the WASH complex is neither a major nor robust interacting protein of VPS35 in the brain, suggesting that it either forms a labile complex with the retromer or that it binds at levels undetectable by our current methods. Despite the lack of WASH complex binding, we do find evidence for a deficiency of VPS35 and WASH complex components in nigral dopaminergic neurons of D620N KI mice. Future studies will be important to determine how the D620N mutation influences VPS35 protein turnover in these neurons and whether or how retromer deficiency is sufficient to induce dopaminergic neurodegeneration. A recent study using a version of this germline D620N KI mouse reports an increase in evoked striatal dopamine release (24), whereas an independent D620N KI model oppositely exhibits impaired dopamine release in young mice (40). These alterations in dopaminergic neurotransmission in young D620N KI mice may indicate an early dysfunction of dopaminergic neurons before their subsequent degeneration at advanced age. Another recent study demonstrates that the D620N mutation in these VPS35 KI mice or in patient-derived human neutrophils and monocytes robustly increases LRRK2-mediated Rab10 phosphorylation (41). These findings suggest that PD-linked *VPS35* mutations may exert their pathogenic actions by increasing LRRK2 kinase activity via an unknown mechanism, which would further lend support to a gain-of-function mechanism for the dominant D620N mutation.

The neuropathological spectrum of PD brains harboring *VPS35* mutations is not yet clear since only a single mutation carrier has so far been evaluated at autopsy (4, 7). Unfortunately, this evaluation lacked an assessment of brain regions of interest, including the substantia nigra, although Lewy pathology was absent from extranigral regions (7). D620N VPS35 KI mice develop robust and widespread tau pathology and axonal damage but lack signs of Lewy pathology positive for α-synuclein. Notably, the viral-mediated overexpression of D620N VPS35 in the nigrostriatal pathway of rats also induces axonal pathology (18). The development of tau pathology in KI mice is reminiscent of familial *LRRK2* mutations. *LRRK2* mutation carriers with PD predominantly develop Lewy pathology but some cases instead exhibit tau pathology in neurons or glial cells (28, 29, 42), whereas numerous mutant LRRK2 rodent models report abnormalities in tau metabolism or phosphorylation as the most consistent pathological feature (27, 43–45). Whether the same is true for *VPS35* mutation carriers is not yet clear, but VPS35 KI mice indicate that the D620N mutation is sufficient for the development of tau abnormalities but not α-synuclein. Notably, the absence of similar tau pathology in heterozygous *VPS35* null mice with age indicates that the D620N mutation exerts this effect via a gain-of-function mechanism. Additional aging up to 24 mo may be required for the development of α-synuclein pathology in the KI mice, or they could potentially develop soluble oligomeric forms of α-synuclein that may not be detectable using the methods applied here. The observation that D620N KI mice are unable to enhance α-synuclein–induced phenotypes that develop in transgenic mice or preformed fibril-based models would tend to argue against meaningful pathological changes in α-synuclein.

Tau pathology can occur in familial and sporadic PD brains albeit much less prominently than Lewy pathology (28, 29, 46). Importantly, common variation in the *MAPT* gene is consistently associated with an increased risk of developing PD and most likely arises through increases in tau transcript expression (30). In the D620N KI mice, tau pathology develops before axonal damage. This could potentially be due to early microtubule instability within axons that would initially lead to tau disassembly from microtubules and its redistribution and accumulation

within somatodendritic compartments of neurons. Inhibition of axonal transport and subsequent axonal damage would likely result from microtubule instability. Our data therefore potentially link abnormal retromer function to microtubule instability but the mechanistic underpinnings remain unclear. These effects could possibly result from the inappropriate recycling of specific axonal cargo by the retromer; however, little is presently known about retromer function and specialized cargo within neurons (47). The recent observation of LRRK2 hyperactivation in D620N VPS35 KI mice could potentially link the microtubule network to tau abnormalities (41), as familial mutations that enhance LRRK2 kinase activity (48, 49) are reported to impair microtubule stability (50, 51), increase tau phosphorylation (52, 53), and promote the neuron-to-neuron transmission of WT tau (54). Alternatively, VPS35 mutations may act upon tau metabolism independent of a primary effect on microtubule stability. For example, the D620N mutation has been suggested to impair the delivery of cathepsin D to the lysosome via the abnormal retromer-dependent endosomal sorting of its receptor, CI-MPR (15, 38), whereas reduced lysosomal cathepsin D is linked to tau-induced neurotoxicity (55). VPS35 mutations could also potentially influence tau-directed kinases, as the hyperphosphorylation of tau is known to reduce its affinity for microtubules and promote their destabilization (26, 31, 56). Future studies should focus on the relationship between *VPS35* mutations and tau pathology, including the mechanism for inducing tau abnormalities and whether tau itself is important for dopaminergic neurodegeneration in the D620N VPS35 KI mice.

Collectively, our data demonstrate that the physiological expression of PD-linked D620N VPS35 in mice is sufficient to recreate the progressive degeneration of nigral dopaminergic neurons that is the major pathological hallmark of familial and sporadic PD. *VPS35* KI mice surprisingly reveal prominent tau pathology, which may represent an important and early feature of mutant VPS35-induced neuronal degeneration in PD. The D620N VPS35 KI mice provide an important tool for elucidating the complex pathophysiological mechanisms underlying neurodegeneration in PD, including the intersection with other important PD genetic risk factors (i.e., *MAPT*/tau and LRRK2).

Materials and Methods

Animals. Mice were maintained in a pathogen-free barrier facility and provided with food and water for ad libitum consumption and exposed to a 12-h light/dark cycle. Animals were treated in strict accordance with the NIH *Guide for the Care and Use of Laboratory Animals* (57). All animal experiments were approved by the Van Andel Institute Animal Care and Use Committee. Conditional ("floxed") *D620N VPS35* KI mice (strain 021807) and CMV-Cre transgenic mice (strain 006054) were obtained from The Jackson Laboratory. Human A53T α-synuclein transgenic mice (line G2-3) have been described (37). Mice were identified by genomic PCR (24, 37).

RNA Extraction and Northern Blot Analysis. Total RNAs were extracted from hemibrains and subjected to Northern blot analysis using a ^{32}P-labeled DNA probe (nucleotides 163–984 of mVPS35). Signal was detected using a Typhoon phosphor-imaging system (Amersham).

Expression Plasmids and Antibodies. Human V5-tagged VPS35 plasmids were obtained from Addgene (no. 21691; ref. 58) and previously described (18). Mouse VPS35 cDNA was obtained from Dharmacon. Primary antibodies used were VPS35 (ab57632 or ab154647; Abcam), VPS26 (ab23892; Abcam), VPS29 (ab10160; Abcam), WASH1 (Sigma), Fam21A-D (S-13; Santa Cruz), V5 and V5-HRP (Life Technologies), TH (NB300-109; Novus Biologicals or clone TH-2; Sigma), α-synuclein (clone 42; BD Biosciences), pSer129-α-synuclein (clone EP1536Y; Abcam), APP (clone 22C11; Millipore), tau (clone Tau5; Millipore), phospho-tau (clones AT8, PHF1, CP13, and MC1, provided by Peter Davies, Feinstein Institute for Medical Research, New York), NeuN (ABN78; Millipore), Iba1 (Wako), GFAP (DAKO), and β-tubulin (clone TUB 2.1; Sigma). Secondary HRP-conjugated IgG, light chain-specific (Jackson Immunoresearch), biotinylated IgG (Vector Labs), and AlexaFluor-488 or -594 IgG (Thermo Fisher) were used.

Cell Culture and Transient Transfection. HEK-293T cells were maintained and transfected using X-tremeGENE HP Reagent (Roche) as described (59).

Co-IP, Western Blotting, and MS. For co-IP assays, hemibrains from 3-mo-old mice or transfected HEK-293T cells were prepared in IP buffer [20 mM Hepes-KOH, pH 7.2, 50 mM potassium acetate, 200 mM sorbitol, 2 mM EDTA, 0.1% Triton X-100, and 1× Complete Mini protease inhibitor mixture (Roche)] and subjected to IP with antibodies to VPS35 or V5 (5 μg) as described (59). IPs and input lysates were subjected to Western blotting, detection, and quantitation as described (59). For MS, anti-VPS35 IPs from WT or VPS35 KI mouse brain were subjected to analysis by nano liquid chromatography/tandem MS (LC-MS/MS) (ThermoFisher Q Exactive) at MS Bioworks as previously described (59).

Sequential Fractionation of Brain Tissues. Brain tissues from KI mice were harvested and subjected to sequential fractionation in low-salt, Triton X-100, and sarkosyl buffers as described previously (54). For standard biochemical analysis, brain tissues were homogenized in lysis buffers containing 1% Triton X-100 or 2% SDS (Triton-insoluble), as described (18, 60).

Measurement of Biogenic Amines. Homogenized tissues were separated on a 150- × 4.6-mm Microsorb MV C18 100-5 column (Agilent Technologies) and analyzed by HPLC-electrochemical detection (ECD) to detect dopamine, HVA, DOPAC, serotonin (5-HT), 5-hydroxyindoleacetic acid (5-HIAA), norepinephrine, and 3-methoxy-4-hydroxyphenylglycol (MHPG), as described previously (61, 62).

Immunohistochemistry and Immunofluorescence. Mice were perfused with 4% paraformaldehyde (pH 7.4), cryoprotected in 30% sucrose, and dissected into 35-μm-thick coronal sections. Immunostaining by incubation with primary and biotinylated secondary antibodies (Vector Labs), ABC reagent (Vector Labs), and DAB (Vector Labs) has been described (18, 60). Images were captured using an Axio Imager M2 (Zeiss) with color CCD camera (AxioCam; Zeiss). Silver staining was conducted on serial sagittal sections using the FD NeuroSilver kit II (FD Neurotechnologies) according to the manufacturer's instructions. Images were captured using a ScanScope XT slide scanner (Aperio) at a resolution of 0.5 μm per pixel. Images were quantified using a custom CellProfiler v3.1.5 pipeline to isolate black neurites and particles. The percent of total pixels associated with black neurites was calculated for each image, sampled across three to six images per animal. Fluorescence immunostaining of brain sections was conducted using primary and secondary antibodies conjugated to AlexaFluor-488 or -594 (Life Technologies), imaged using a Nikon A1plus-RSi Laser Scanning Confocal microscope (Nikon Instruments), and subjected to quantitation by corrected total cellular fluorescence (CTCF) as previously described (59). CTCF values were derived by sampling across five sections per animal for hippocampal subregions, or from ≥40 TH-positive neurons per animal for the SNpc.

Stereological Analysis and Optical Densitometry. Unbiased stereological quantitation of SNpc dopaminergic neurons was performed using the optical fractionator probe of StereoInvestigator software (MicroBrightField Biosciences), as previously described (18, 60). The optical density of TH-immunoreactive nerve terminals in the striatum was determined using the ScanScope XT slide scanner (Aperio) and optical densitometry using NIH ImageJ (v1.3). The mean optical density across six to eight sections per animal was determined.

Stereotactic Delivery of Preformed Fibrils. Mouse α-synuclein was expressed in *Escherichia coli* and purified as previously described (63). To generate fibrils, 5 mg/mL of purified α-synuclein in 1× PBS, pH 7.4, was shaken at 1,000 rpm for 7 d, sonicated with 60 pulses at 10% power (30 s total time, 0.5 s on, 0.5 s off), aliquoted, and stored at −80 °C. Sedimentation assays and thioflavin T assays were performed as described (63, 64) to ensure fibril quality. Male adult littermate mice (n = 3 mice per genotype) were subjected to stereotactic surgery for the unilateral delivery of PFF-αSyn into the dorsal striatum. The following coordinates were used relative to bregma: anterior–posterior, +0.2 mm; medial–lateral, +2.0 mm; and dorsal–ventral, −2.6 mm. Mice received PFF-αSyn (5 μg) in 1 μL at a flow rate of 0.1 μL/min. Animals were euthanized at 30 d postinjection.

Behavioral Assessments. Behavioral testing was performed on male and female mice at ages indicated for each test, as described (60). Open-field testing using an Ethovision XT video tracking system (Noldus Information Technology), accelerating rotarod (5 to 50 rpm over 5 min), and digital Gait analysis using the automated CatWalk XT system (Noldus) were conducted.

1. Hernandez DG, Reed X, Singleton AB (2016) Genetics in Parkinson disease: Mendelian versus non-Mendelian inheritance. *J Neurochem* 139:59–74.
2. Lang AE, Lozano AM (1998) Parkinson's disease. Second of two parts. *N Engl J Med* 339:1130–1143.
3. Lang AE, Lozano AM (1998) Parkinson's disease. First of two parts. *N Engl J Med* 339:1044–1053.
4. Vilariño-Güell C, et al. (2011) VPS35 mutations in Parkinson disease. *Am J Hum Genet* 89:162–167.
5. Zimprich A, et al. (2011) A mutation in VPS35, encoding a subunit of the retromer complex, causes late-onset Parkinson disease. *Am J Hum Genet* 89:168–175.
6. Williams ET, Chen X, Moore DJ (2017) VPS35, the retromer complex and Parkinson's disease. *J Parkinsons Dis* 7:219–233.
7. Wider C, et al. (2008) Autosomal dominant dopa-responsive parkinsonism in a multigenerational Swiss family. *Parkinsonism Relat Disord* 14:465–470.
8. Seaman MN (2004) Cargo-selective endosomal sorting for retrieval to the Golgi requires retromer. *J Cell Biol* 165:111–122.
9. Seaman MN (2012) The retromer complex–endosomal protein recycling and beyond. *J Cell Sci* 125:4693–4702.
10. Seaman MNM, Marcusson EG, Cereghino JL, Emr SD (1997) Endosome to Golgi retrieval of the vacuolar protein sorting receptor, Vps10p, requires the function of the VPS29, VPS30, and VPS35 gene products. *J Cell Biol* 137:79–92.
11. Seaman MNM, McCaffery JM, Emr SD (1998) A membrane coat complex essential for endosome-to-Golgi retrograde transport in yeast. *J Cell Biol* 142:665–681.
12. Bonifacino JS, Hurley JH (2008) Retromer. *Curr Opin Cell Biol* 20:427–436.
13. Hierro A, et al. (2007) Functional architecture of the retromer cargo-recognition complex. *Nature* 449:1063–1067.
14. Seaman MN, Gautreau A, Billadeau DD (2013) Retromer-mediated endosomal protein sorting: All WASHed up! *Trends Cell Biol* 23:522–528.
15. Follett J, et al. (2014) The Vps35 D620N mutation linked to Parkinson's disease disrupts the cargo sorting function of retromer. *Traffic* 15:230–244.
16. McGough IJ, et al. (2014) Retromer binding to FAM21 and the WASH complex is perturbed by the Parkinson disease-linked VPS35(D620N) mutation. *Curr Biol* 24:1670–1676, and erratum (2014) 24:1678.
17. Munsie LN, et al. (2014) Retromer-dependent neurotransmitter receptor trafficking to synapses is altered by the Parkinson's disease VPS35 mutation p.D620N. *Hum Mol Genet* 24:1691–1703.
18. Tsika E, et al. (2014) Parkinson's disease-linked mutations in VPS35 induce dopaminergic neurodegeneration. *Hum Mol Genet* 23:4621–4638.
19. Zavodszky E, et al. (2014) Mutation in VPS35 associated with Parkinson's disease impairs WASH complex association and inhibits autophagy. *Nat Commun* 5:3828.
20. Tian Y, et al. (2015) VPS35-deficiency results in an impaired AMPA receptor trafficking and decreased dendritic spine maturation. *Mol Brain* 8:70.
21. Tang FL, et al. (2015) VPS35 in dopamine neurons is required for endosome-to-Golgi retrieval of Lamp2a, a receptor of chaperone-mediated autophagy that is critical for α-synuclein degradation and prevention of pathogenesis of Parkinson's disease. *J Neurosci* 35:10613–10628.
22. Tang FL, et al. (2015) VPS35 deficiency or mutation causes dopaminergic neuronal loss by impairing mitochondrial fusion and function. *Cell Rep* 12:1631–1643.
23. Wen L, et al. (2011) VPS35 haploinsufficiency increases Alzheimer's disease neuropathology. *J Cell Biol* 195:765–779.
24. Cataldi S, et al. (2018) Altered dopamine release and monoamine transporters in Vps35 p.D620N knock-in mice. *NPJ Parkinsons Dis* 4:27.
25. Lee VM, Goedert M, Trojanowski JQ (2001) Neurodegenerative tauopathies. *Annu Rev Neurosci* 24:1121–1159.
26. Wang Y, Mandelkow E (2016) Tau in physiology and pathology. *Nat Rev Neurosci* 17:5–21.
27. Islam MS, Moore DJ (2017) Mechanisms of LRRK2-dependent neurodegeneration: Role of enzymatic activity and protein aggregation. *Biochem Soc Trans* 45:163–172.
28. Zimprich A, et al. (2004) Mutations in LRRK2 cause autosomal-dominant parkinsonism with pleomorphic pathology. *Neuron* 44:601–607.
29. Rajput A, et al. (2006) Parkinsonism, Lrrk2 G2019S, and tau neuropathology. *Neurology* 67:1506–1508.
30. Nalls MA, et al.; International Parkinson's Disease Genomics Consortium (IPDGC); Parkinson's Study Group (PSG) Parkinson's Research: The Organized GENetics Initiative (PROGENI); 23andMe; GenePD; NeuroGenetics Research Consortium (NGRC); Hussman Institute of Human Genomics (HIHG); Ashkenazi Jewish Dataset Investigator; Cohorts for Health and Aging Research in Genetic Epidemiology (CHARGE); North American Brain Expression Consortium (NABEC); United Kingdom Brain Expression Consortium (UKBEC); Greek Parkinson's Disease Consortium; Alzheimer Genetic Analysis Group (2014) Large-scale meta-analysis of genome-wide association data identifies six new risk loci for Parkinson's disease. *Nat Genet* 46:989–993.
31. Iqbal K, Liu F, Gong CX (2016) Tau and neurodegenerative disease: The story so far. *Nat Rev Neurol* 12:15–27.
32. Spillantini MG, Crowther RA, Jakes R, Hasegawa M, Goedert M (1998) Alpha-synuclein in filamentous inclusions of Lewy bodies from Parkinson's disease and dementia with lewy bodies. *Proc Natl Acad Sci USA* 95:6469–6473.
33. Spillantini MG, et al. (1997) Alpha-synuclein in Lewy bodies. *Nature* 388:839–840.
34. Singleton AB, et al. (2003) Alpha-synuclein locus triplication causes Parkinson's disease. *Science* 302:841.
35. Dhungel N, et al. (2015) Parkinson's disease genes VPS35 and EIF4G1 interact genetically and converge on α-synuclein. *Neuron* 85:76–87.
36. Fujiwara H, et al. (2002) Alpha-synuclein is phosphorylated in synucleinopathy lesions. *Nat Cell Biol* 4:160–164.
37. Lee MK, et al. (2002) Human alpha-synuclein-harboring familial Parkinson's disease-linked Ala-53–> Thr mutation causes neurodegenerative disease with alpha-synuclein aggregation in transgenic mice. *Proc Natl Acad Sci USA* 99:8968–8973.
38. Miura E, et al. (2014) VPS35 dysfunction impairs lysosomal degradation of α-synuclein and exacerbates neurotoxicity in a Drosophila model of Parkinson's disease. *Neurobiol Dis* 71:1–13.
39. Wang W, et al. (2016) Parkinson's disease-associated mutant VPS35 causes mitochondrial dysfunction by recycling DLP1 complexes. *Nat Med* 22:54–63.
40. Ishizu N, et al. (2016) Impaired striatal dopamine release in homozygous Vps35 D620N knock-in mice. *Hum Mol Genet* 25:4507–4517.
41. Mir R, et al. (2018) The Parkinson's disease VPS35[D620N] mutation enhances LRRK2-mediated Rab protein phosphorylation in mouse and human. *Biochem J* 475:1861–1883.
42. Ross OA, et al. (2006) Lrrk2 and Lewy body disease. *Ann Neurol* 59:388–393.
43. Li X, et al. (2010) Enhanced striatal dopamine transmission and motor performance with LRRK2 overexpression in mice is eliminated by familial Parkinson's disease mutation G2019S. *J Neurosci* 30:1788–1797.
44. Li Y, et al. (2009) Mutant LRRK2(R1441G) BAC transgenic mice recapitulate cardinal features of Parkinson's disease. *Nat Neurosci* 12:826–828.
45. Melrose HL, et al. (2010) Impaired dopaminergic neurotransmission and microtubule-associated protein tau alterations in human LRRK2 transgenic mice. *Neurobiol Dis* 40:503–517.
46. Mattila PM, Röyttä M, Torikka H, Dickson DW, Rinne JO (1998) Cortical Lewy bodies and Alzheimer-type changes in patients with Parkinson's disease. *Acta Neuropathol* 95:576–582.
47. Choy RW, et al. (2014) Retromer mediates a discrete route of local membrane delivery to dendrites. *Neuron* 82:55–62.
48. West AB, et al. (2005) Parkinson's disease-associated mutations in leucine-rich repeat kinase 2 augment kinase activity. *Proc Natl Acad Sci USA* 102:16842–16847.
49. Steger M, et al. (2016) Phosphoproteomics reveals that Parkinson's disease kinase LRRK2 regulates a subset of Rab GTPases. *eLife* 5:e12813.
50. Godena VK, et al. (2014) Increasing microtubule acetylation rescues axonal transport and locomotor deficits caused by LRRK2 Roc-COR domain mutations. *Nat Commun* 5:5245.
51. Kett LR, et al. (2012) LRRK2 Parkinson disease mutations enhance its microtubule association. *Hum Mol Genet* 21:890–899.
52. Bailey RM, et al. (2013) LRRK2 phosphorylates novel tau epitopes and promotes tauopathy. *Acta Neuropathol* 126:809–827.
53. Kawakami F, et al. (2012) LRRK2 phosphorylates tubulin-associated tau but not the free molecule: LRRK2-mediated regulation of the tau-tubulin association and neurite outgrowth. *PLoS One* 7:e30834.
54. Nguyen APT, et al. (2018) G2019S LRRK2 enhances the neuronal transmission of tau in the mouse brain. *Hum Mol Genet* 27:120–134.
55. Khurana V, et al. (2010) Lysosomal dysfunction promotes cleavage and neurotoxicity of tau in vivo. *PLoS Genet* 6:e1001026.
56. Kneynsberg A, Kanaan NM (2017) Aging does not affect axon initial segment structure and somatic localization of tau protein in hippocampal neurons of fischer 344 rats. *eNeuro* 4:ENEURO.0043-17.2017.
57. National Research Council (2011) *Guide for the Care and Use of Laboratory Animals* (National Academies Press, Washington, DC), 8th Ed.
58. Scott KL, et al. (2009) GOLPH3 modulates mTOR signalling and rapamycin sensitivity in cancer. *Nature*, 459, pp 1085–1090.
59. Williams ET, et al. (2018) Parkin mediates the ubiquitination of VPS35 and modulates retromer-dependent endosomal sorting. *Hum Mol Genet* 27:3189–3205.
60. Tsika E, et al. (2014) Conditional expression of Parkinson's disease-related R1441C LRRK2 in midbrain dopaminergic neurons of mice causes nuclear abnormalities without neurodegeneration. *Neurobiol Dis* 71:345–358.
61. Kanaan NM, et al. (2015) The longitudinal transcriptomic response of the substantia nigra to intrastriatal 6-hydroxydopamine reveals significant upregulation of regeneration-associated genes. *PLoS One* 10:e0127768.
62. Perez SE, et al. (2005) Nigrostriatal dysfunction in familial Alzheimer's disease-linked APPswe/PS1DeltaE9 transgenic mice. *J Neurosci* 25:10220–10229.
63. Becker K, et al. (2018) Detecting alpha synuclein seeding activity in formaldehyde-fixed MSA patient tissue by PMCA. *Mol Neurobiol* 55:8728–8737.
64. Volpicelli-Daley LA, Luk KC, Lee VM (2014) Addition of exogenous α-synuclein preformed fibrils to primary neuronal cultures to seed recruitment of endogenous α-synuclein to Lewy body and Lewy neurite-like aggregates. *Nat Protoc* 9:2135–2146.